Dynamic fusion of genomics and functional network connectivity in UK biobank reveals static and time-varying SNP manifolds

Jiayu Chen[1,2], Armin Iraji[1,2], Zening Fu[1], Pablo Andrés-Camazón[3], Bishal Thapaliya[1], Jingyu Liu[1,2,†], Vince D. Calhoun[1,2,†]

[1]Tri-Institutional Center for Translational Research in Neuroimaging and Data Science (TReNDS): (Georgia State University, Georgia Institute of Technology, and Emory University), Atlanta, GA, USA; [2]Department of Computer Science, Georgia State University, Atlanta, GA, USA; [3]Department of Child and Adolescent Psychiatry, Institute of Psychiatry and Mental Health, Hospital General Universitario Gregorio Marañón, IiSGM, Madrid, Spain

[†]Contributing equally.

*Corresponding authors:

Vince D. Calhoun, 55 Park Pl NE, Atlanta, GA 30303, vcalhoun@gsu.edu

Running title: Dynamic fusion of SNP and FNC

ABSTRACT

Many psychiatric and neurological disorders show significant heritability, indicating strong genetic influence. In parallel, dynamic functional network connectivity (dFNC) measures functional temporal coupling between brain networks in a time-varying manner and has proven to identify disease-related changes in the brain. However, it remains largely unclear how genetic risk contributes to brain dysconnectivity that further manifests into clinical symptoms. The current work aimed to address this gap by proposing a novel joint ICA (jICA)-based "dynamic fusion" framework to identify dynamically tuned SNP manifolds by linking static SNPs to dynamic functional information of the brain. The sliding window approach was utilized to estimate four dFNC states and compute subject-level state-specific dFNC features. Each state of dFNC features were then combined with 12946 SZ risk SNPs for jICA decomposition, resulting in four parallel fusions in 32861 European ancestry individuals within the UK Biobank cohort. The identified joint SNP-dFNC components were further validated for SZ relevance in an aggregated SZ cohort, and compared for across-state similarity to indicate level of dynamism. The results supported that dynamic fusion yielded "static" and "dynamic" components (i.e., high and low across-state similarity, respectively) for SNP and dFNC modalities. As expected, the SNP components presented a mixture of static and dynamic manifolds, with the latter largely driven by fusion with dFNC. We also showed that some of the dynamic SNP manifolds uniquely elicited by fusion with state-specific dFNC features complemented each other in terms of biological interpretation. This dynamic fusion framework thus allows expanding the SNP modality to manifolds in the time dimension, which provides a unique lens to elicit unique SNP correlates of dFNC otherwise unseen, promising additional insights on how genetic risk links to disease-related dysconnectivity.

INTRODUCTION

It has been well established that many psychiatric and neurological disorders show significant heritability[1-4]. Family and twin studies have suggested heritability rates ranging from 0.80 for schizophrenia (SZ)[1], to 0.90 for autism (ASD)[5], and 0.60-0.80 for Alzheimer's disease (AD)[6]. More recently, large-scale genome-wide association studies (GWASs) have opened a new chapter of characterizing genomic profiles underlying complex brain disorders, confirming the polygenic nature and quantifying the contribution of common genetic variants to heritability[7,8]. Despite not accounting for all the heritability as implicated in family data, significant estimates have been consistently reported across studies for common-variant-based heritability, varying from 0.10 for AD to 0.28 for obsessive compulsive disorder (OCD), and consistently 0.23-0.24 for SZ[8,9]. It is thus of great clinical significance to understand how genetic factors impact predisposition, disease progression, and response to treatment, which is expected to facilitate personalized health care and precision medicine[10-12].

A common notion is that in brain disorders, genetic factors exert influence on clinical manifestations by affecting the brain. A full delineation of pathophysiological pathways involves genetic underpinnings, environmental factors, brain phenotypes, and clinical symptoms. The past decade has seen great efforts to decipher brain disorders by characterizing their genetic risk and related brain abnormalities, known as imaging genomics[13], so that a specific disorder may be described from a multi-scale multi-dimensional perspective for a comprehensive understanding of its underlying biology[14-16]. The hope is that such a dimensional framework would allow detecting and quantifying risk at an early stage and stratifying individuals based on biological underpinnings, ultimately leading to more efficient individualized treatment[17,18].

The task of identifying and understanding the genetic and neurobiological profiles and their relationships in complex brain disorders has proved to be a challenge, despite initial expectations. Given their polygenic nature, the heritability is distributed across a large number of genetic variants with modest

effect sizes, which resonated with distributed rather than focal abnormalities at the neurobiological level. Consequently, imaging genomic studies usually suffer high dimensionality and insufficient statistical power. Many multivariate approaches have been proposed to address these issues as reviewed in[19], largely falling into (a) dimensionality reduction, as represented by the family of data decomposition approaches, including principal components analysis (PCA), independent component analysis (ICA), joint ICA, parallel ICA, and non-negative matrix factorization (NMF); and (b) imposing sparsity constraint as implemented in sparse canonical component analysis (CCA), sparse partial least square regression (PLS), sparse reduced rank regression, and sparse ICA. Some of the listed approaches also highlight data fusion to enhance intercorrelations between imaging and genetic modality, such as parallel ICA, sparse CCA, sparse PLS[20-23], as well as those incorporating deep learning techniques such as deep CCA[24,25]. In parallel to mathematical modeling, unprecedented large-scale GWASs offer another strategy of dimensionality reduction to admit only disease-relevant variants into analysis[26-29]. In addition, with data sharing gaining ground, more resources have become available to promise improved power through data aggregation. Particularly, previous work has shown many cases where the examined genomic risk variants presented similar effects on the brain in disease and healthy populations (i.e., no significant disease interaction)[30-32]. Significant associations have also been noted between polygenic risk scores (PRS) for SZ and various brain measures, including frontal and temporal structural measures, subcortical brain volumes, and neural flexibility and network modularity during a working memory task, in large population cohorts such as UK Biobank (UKB)[33-35]. Collectively, it is well-grounded and motivated to leverage large population cohorts to investigate the interrelationships between disease-related genetic and neurobiological factors.

Dynamic functional network connectivity (dFNC) measures functional temporal coupling between brain networks in a time-varying manner and has proven to identify disease-related changes in the brain[36-38]. Compared to static FNC (sFNC), dFNC provides richer information that describes how functional interactions vary across time, rather than assuming the interaction remains the constant for the whole period. One commonly utilized strategy to characterize dFNC is the sliding window approach, which

obtains a sequence of window FNCs (wFNCs) by localizing the data through a sliding window[39]. The temporal dynamics can then be described as a flow between wFNC patterns to yield summary features and statistics, and to allow estimating stable representative connectivity patterns, known as dFNC states[40,41], for further investigation on clinical relevance[36,42]. The dFNC approach has proven to yield highly informative neurobiological markers for disease discrimination, e.g., classifying schizophrenia, bipolar disorder, autism, and mild traumatic brain injury[43-45], and significantly outperformed sFNC in classifying patients with SZ and bipolar disorder [43].

While dFNC effectively captures disease-related dysconnectivity, the knowledge about its genetic correlates is still very limited. The GWASs of brain imaging phenotypes conducted on the UKB data indicate that despite not showing as high heritability as structural phenotypes, 235 out of 1771 tested functional connectivity pairs showed significant heritability[46]. In addition, when ICA was applied on the 1771 connectivity pairs, the resulting connectivity components showed much stronger heritability[46]. These observations motivate further elucidations on genetic profiles underlying functional connectivity, particularly those disrupted in SZ. One previous work explored linking genetic variants with dFNC using parallel ICA, where all the dFNC states were concatenated to form a feature matrix and investigated for associations with SZ-related single nucleotide polymorphisms (SNPs)[47]. This implementation is more likely to highlight genetic associations with those dFNC features showing similar subject-level variations across all the states, while the subject-level variations more unique to individual dFNC states are less represented.

The current work aimed to address this gap by proposing a novel joint ICA (jICA)-based "dynamic fusion" framework to compare manifolds of SNP-fMRI association across parallel data fusion between SZ risk SNPs and individual dFNC states. The most recent psychiatric genomic consortium GWAS of SZ was leveraged to select out SNPs conferring risk for SZ[27], which were then jointly analyzed with dFNC features estimated using the NeuroMark pipeline[48] in 32,861 European ancestry individuals within the UKB cohort. The identified joint SNP-dFNC components were further investigated for SZ relevance in an

aggregated SZ cohort. We hypothesized that the joint SNP-dFNC components would show different levels of across-state similarity. Given the previous work[47], it was expected that certain FNC pairs would cluster in a similar way across all the states, leading to components showing higher similarity across states, or low dynamism. Meanwhile, the jICA-based dynamic fusion framework allows us to capture state-specific clusters of FNC pairs, or high-dynamism dFNC components. For the SNP modality, given the static input, we expected the components to present a mixture of static and dynamic patterns, with the latter largely driven by fusion with dFNC. That is, we aimed to estimate dynamically tuned SNP manifolds from static SNP data by linking it to dynamic functional information of the brain. We would evaluate modality-specific similarity across the parallel fusions to verify the hypothesis. To our knowledge, this is the first work comparing the dynamic or static nature of the decompositions across multiple data fusions. This dynamic fusion framework thus provides a unique lens that may elicit unique SNP correlates missed in previous work, providing additional insights on how genetic risk links to SZ-related dysconnectivity.

MATERIALS AND METHODS

Participants

UK Biobank. The current work leveraged the population-based UKB cohort which recruited more than 500K individuals across the United Kingdom. The UKB study was approved by the North West Haydock Research Ethics Committee, and the data used in our work were obtained under data application number 34175. Specifically, we used the imputed SNP data and resting-state functional magnetic resonance images (rsfMRI) of 32681 European ancestry individuals with both imaging and genetic modalities available after quality control (QC, detailed below), including 15357 males and 17504 females, aged between 45-81 with a median of 64 when brain MRI was collected.

SZ cohorts. Additional SZ cohorts were utilized to validate the UKB findings for SZ relevance. For this purpose, four SZ cohorts were aggregated to boost power, including COBRE[49], FBIRN[38], B-SNIP1[50],

and MPRC[51], resulting in 1237 individuals with rsfMRI data after QC, including 528 individuals with SZ and 709 controls (740 males and 497 females, aged between 16-79 with a median of 38). The institutional review board at each site approved the study and all participants provided written informed consent. Details regarding recruitment and data collection can be found in previous publications[38,51-54].

SNP preprocessing and pre-screening

SNP data. The imputed SNP data released by UKB consisted of 487,320 individuals and ~96 million variants (v3_s487320). Details of genotyping and imputation can be found in the paper that describes the UKB genomic data[55]. In brief, DNA was extracted from blood samples and genotyping was carried out by Affymetrix Research Services Laboratory. Most of the individuals (94%) reported their ethnic background as 'white,' which was a broad-level group. SHAPEIT3 was used for phasing[56]. Imputation was conducted using IMPUTE4[55] with the Haplotype Reference Consortium reference panel[57] and the UK10K Consortium reference panel[58].

Preprocessing of SNP. In this study, we first identified the participants that passed the UKB quality control (sex mismatch, missing rate, and heterozygosity) and also had rsfMRI data available. We then excluded SNPs with minor allele frequencies < 0.01, as recommended for subsequent GWAS and PRS analysis[59]. We then conducted relatedness estimation (identify-by-descent) using PLINK[60]. For each group of individuals that were second-degree relatives or closer, only one individual was retained for subsequent analysis. Finally, we identified individuals of European ancestry (in a stricter sense) to be those close (< 3SD) to the center of the 'white' cluster as defined by the first four principal components.

Pre-screening. We then selected SZ risk SNPs based on the 287 loci identified by PGC SCZ2022[27], which were further pruned at $r^2 < 0.2$, resulting in a total of 12946 SNPs included in the dynamic fusion analysis.

Estimation of dFNC

Resting-state fMRI data. While the UKB imaging enhancement plan aims to re-invite 100K participants for multi-modal imaging, the data we obtained contain rsfMRI scans of ~38K individuals. UKB used identical scanner models, coils, software, and protocols across centers to ensure data harmonization as much as possible[61]. The rsfMRI scan parameters are as follows: resolution = 2.4 mm × 2.4 mm × 2.4 mm, matrix = 88 × 88 × 64, TE = 39 ms, TR = 735 ms, alpha = 51°, multi-band factors = 8, duration = 6:10 mins [61]. For the SZ cohorts, detailed scanning parameters can be found in supplemental text 1 (**ST1)**.

Preprocessing of rsfMRI. We downloaded the preprocessed UKB data, and normalized the images to standard MNI space (http://www.mni.mcgill.ca/) and resampled to 3 mm × 3 mm × 3 mm voxels using the SPM nonlinear registration, followed by smoothing using a 6mm FWHM Gaussian kernel. The rsfMRI data of the SZ cohorts were preprocessed using the fully automated NeuroMark pipeline (SPM12-based) established[48,62]. The first 10 dummy volumes were discarded to guarantee tissue reaches a steady state of radiofrequency excitation. Slice-time correction was applied using the middle slice as the reference frame. After the slicing timing, subject head motions were corrected by the realignment function in SPM12. Subjects with maximum translation of head motion greater than 3 mm or the rotation of head motion exceeding 3° in any axe were excluded. The preprocessed images were then normalized, resampled and smoothed in a same way as for UKB.

Estimation of windowed FNC. The Neuromark_fMRI_1.0 network template[48,62] served as a reference in a spatial-constrained independent component analysis (scICA) [63] to derive 53 subject-level intrinsic connectivity networks (ICNs) and their associated time courses (TCs). The subject-level TCs then went through addition processing steps, including detrending, despiking, regressions of the six realignment parameters and their temporal derivatives, and band-pass filtering with 0.01–0.15 Hz. Windowed FNC (wFNC) was then estimated based on the processed TCs of 53 ICNs as described in our previous work[36,48]. In brief, a tapered sliding window (convolving a rectangular window of 20 TRs was

used to estimate covariance from the regularized precision matrix, resulting in a sequence of wFNCs of 1378 FNC pairs for each individual with the UKB and SZ cohorts.

Estimation of dFNC states. Dynamic FNC states were then estimated from the UKB data. The wFNCs of all UKB individuals were concatenated, on which K-means clustering with Euclidean distance was applied to identify clusters of similar connectivity patterns across time windows and individuals, or dFNC states. In the current work, we identified four dynamic states, where the optimal number of states was determined as four based on the elbow method.

Subject-level dFNC features. For all the individuals in both UKB and SZ data, we assigned each of wFNCs to the nearest dFNC state based on its Euclidean distance to the state centroid. For each individual, wFNCs assigned to the same state were averaged to yield the most representative FNC patterns of this individual in a dynamic state, denoted as subject-specific state-average dFNC in the following text. In total, four sets of subject-specific state-average dFNCs were generated and used in the fusion analysis. It should be noted that some individuals might not have experienced all four states during the length of scan. We therefore allowed varying sample sizes across states. As a result, 31814/32775/17929/27497 individuals were utilized for SNP fusion with states 1/2/3/4, respectively in UKB, and 1018/1199/954/788 individuals were used for the SZ data to validate the dFNC findings for each state.

Fusion by Joint ICA. Figure 1 shows the diagram of dynamic fusion, which involved linking the same SZ risk SNPs separately with each state-average dFNC via a SNP-dFNC jICA[64]. Joint ICA builds upon Infomax ICA which achieves data decomposition by detecting features covarying with each other and clustering them into components following super-Gaussian distributions[65]. In this sense, applying jICA to fused SNP-dFNC data is expected to capture maximally independent patterns of SNPs and dFNCs that vary similarly across individuals and group them into the same component, thus revealing the linkage between the two modalities. By decomposition $\mathbf{X} = \mathbf{AS}$, jICA decomposed the data $\mathbf{X}$ (i.e., fused

data matrix of X_{SNP} and X_{dFNC}) into a linear combination of a set of source components (**S**) and their associated loadings (**A**). Each source component largely reflects how individual features are linearly weighted to collectively define the loading, which can be interpreted as the most representative subject-level variation pattern shared among those features heavily weighted for this component. Specifically in this work, we conducted four SNP-dFNC fusions on the UKB data, as shown in Figure 1. Each data modality was first normalized by the matrix root mean square. Then the two feature matrices (12946 SNPs and 1378 connectivity edges) were concatenated horizontally into a 32861 × 14324 matrix for decomposition by jICA (Infomax)[65]. The component number was estimated to be 35 based on the PCA scree plot. As a result, we obtained four sets of SNP-dFNC joint components, one set for the fusion of SNPs with one state-average dFNC.

While Infomax ICA is expected to yield super-Gaussian components, we rationalized that it would be an indicator of balanced data fusion if both the SNP and dFNC part of the joint components (referred to as SNP and dFNC components in the following text) showed super-Gaussian histograms, rather than one modality dominating and the other modality under-represented in the data decomposition. Consequently, we conducted post-jICA QC to inspect the histogram and kurtosis of SNP and dFNC for each joint component. Those components with double-peaked SNP or dFNC histograms or with histogram kurtosis < 3 were excluded from the subsequent analysis.

SZ relevance. While the SZ-relevance of SNPs was supported by the GWAS, the relevance of dFNC findings to SZ remained to be validated. For this purpose, we projected the dFNC components onto the state-average dFNC features of the aggregated SZ data by: $A^{SZ} = X^{SZ} {S_{dFNC}^{UKB}}^{-1}$. The underlying assumption was that the connectivity patterns or connectome as characterized by the components were expected to generalize to new data, which allowed us to compute the loadings defined by the same linear combination of dFNC features. The resulting loadings (A_{SZ}) were then investigated for differences between patients with SZ and controls using a two-sample t-test, controlling for age, sex, and dummy-

coded site variables. Significant SZ-discriminating dFNC components were identified with FDR-corrected $p < 0.05$ across all the four sets of components.

Interpretation of joint components. First, we evaluated the components' across-state similarity (Figure 1). For each SNP-dFNC component of a specific state, we identified the most similar SNP and dFNC components with the largest correlations in each of the other three states and computed the average of the three largest correlations to measure the overall SNP and dFNC across-state similarity. Lower similarity indicated higher state-specificity or dynamism, as the connectivity pattern captured by the component was likely varying more across time . Second, for all the joint components whose dFNC features showed significant SZ discrimination, we conducted further analysis to understand their biological implications. The components were thresholded at |z-score| > 3 for heavily weighted SNP and dFNC features that were more tightly coupled with each other. For each component, the top dFNC features comprised a set of FNC pairs that were in concert and could be interpreted based on the anatomical labels of ICNs involved in the connectome. In parallel, the top SNPs were annotated to genes and investigated for enrichment in biological processes using gene ontology [66].

RESULTS

We obtained four sets of joint SNP-dFNC components from the parallel dynamic fusion, each set consisting of 35 components extracted by jICA after fusing the 12946 SZ risk SNPs with one of the four state-average dFNC features (1,378 connectivity pairs). A total of nine components with either double-peaked SNP/dFNC histograms or kurtosis < 3 were eliminated by the post-jICA QC. For the remaining 131 components across the four parallel fusions, the SNP modality showed higher average kurtosis than the dFNC modality (169.84 vs. 8.61). The dFNC part of these components were then projected onto the SZ cohort, of which 53 components were validated as SZ-relevant by showing significant case-control differences, as summarized in Table 1, where the percentage of explained variance (r^2) ranged between 0.46% and 8.18%. For each component, the paired component with top overall similarity in parallel

fusions was also listed, along with the SNP and dFNC component similarities observed in the paired component.

The top SNPs and dFNC features of SZ-relevant components were identified as those with |z-score| > 3. Supplemental Table 1 provides a list of the genes annotated to the top SNPs of individual SZ-relevant components. The top dFNC features (i.e., connectivity pairs) were characterized by the anatomical labels of the two involved ICNs, as summarized in supplemental Table 2. In addition, Manhattan and connectogram plots were generated for the SNP and dFNC components respectively (see supplemental file). Finally, we conducted pathway analysis on the annotated genes using gene ontology. For those SNP components where a significant enrichment existed, we summarized the involved major biological processes in Table 2.

Figure 2 shows the components' dynamism as measured by across-state similarity, which were computed separately for SNP and dFNC, and plotted in a sorted manner for each state. Note that for a joint component, its SNP and dFNC part might present different levels of across-state similarity and be located in different positions in these plots. Overall the components showed a wide range of dynamism for both SNP and dFNC. The SZ-relevant components were highlighted by asterisks, which did not appear to be enriched in the high or low dynamism end.

For illustrative purposes, Figures 3 and 4 show two pairs of SZ-relevant components as examples that overall presented intermediate levels of similarity. Figure 3 presents component 9 of SNP-dFNC$_{state1}$ fusion (denoted as State1_jICA9) which showed similar patterns as State3_jICA7. The left panel of Figure 3 shows the Manhattan plots of the SNP parts of these two components, with dashed lines indicating the threshold of |z-score > 3| for top SNPs. An overlapping ratio of 37% was noted between the annotated genes of these two SNP components. As shown in Table 2, both State1_jICA9 and State3_jICA7 were significantly enriched for regulation of cell projection organization. Other enriched pathways included synaptic plasticity, learning, and memory for State1_jICA9, and cell signaling and

system development for State3_jICA7. The right panel shows the connectograms of the dFNC parts, which also showed similar connectivity patterns to highlight thalamus and subthalamus/hypothalamus connections to other ICNs (see supplemental Table 2 for labels of the top connectivity edges).

State1_jICA13 and State3_jICA5 make another pair of joint components that showed an intermediate level of similarity. The Manhattan plots and connectograms are shown in Figure 4. An overlapping ratio of 31% was observed between the top genes. State1_jICA13 was significantly enriched in neuron projection, synapse organization, and calcium ion transport, while State3_jICA5 was enriched in regulation of lyase activity. Both dFNC components highlighted cerebellum connections to other ICNs.

Figure 5 presents the Manhattan plot and connectograms of State1_jICA30 (lower left connectogram) and State2_jICA32 (lower right connectogram), serving as an example of joint components with very high across-state similarity in SNPs. Only the SNP component of State1_jICA30 was plotted in Figure 5 to avoid redundancy, which was sparse and reflected the effects of a small set of SNPs in chromosome 8. The annotated three genes were 100% overlapping, for which no significant pathway enrichment was noted. In contrast to the high SNP similarity, the dFNC components showed an intermediate level of similarity. Despite not sharing top dFNC features, when thresholded at |z-score| > 2, these two components showed similar connections between cognitive control (CC) and default mode network (DMN) ICNs.

Finally, Figure 6 shows two examples of components with low across-state similarity, and therefore considered as more dynamic. The upper panel highlights State1_jICA4, whose SNP component was significantly enriched for regulation of cell projection, and the dFNC component reflected insula connections to other ICNs. Another highly dynamic component State1_jICA6 was illustrated in the lower panel of Figure 6. Its SNP part was found to be significantly enriched for neurogenesis and synaptic plasticity with the dFNC part capturing connections of the middle temporal gyrus (MTG) with other ICNs.

DISCUSSION

The current work investigates whether the dynamic fusion of SNPs and FNC features brings additional insights into how genetic risk links to SZ-related dysconnectivity. For this purpose, we estimated dFNC states using the established NeuroMark pipeline and computed the state-specific dFNC features. Then four multimodal fusion analyses were conducted on SZ-risk SNPs and dFNC features of each of the four states using joint ICA. By data decomposition, we obtained four sets of SNP-dFNC joint components, which allowed us to measure the modality-specific similarity of individual components across the four parallel fusions, and further interpret whether this dynamic fusion framework elicited unique imaging-genomic factors missed in previous work.

As expected, both SNP and dFNC components yielded by dynamic fusions showed a wide range of across-state similarity, while differences were also noted between the two modalities. As shown in Figure 2, the SNP modality reached higher similarity compared to dFNC and also showed more sharp decreases in similarity while more dFNC components presented an intermediate level of similarity. The high similarity SNP components were in general accompanied by dFNC components with intermediate to low similarity, and typically highlighted a small set of top genes and connectivity edges, as shown in Figure 5 for an example. We interpret this type of joint component as modality-static localized genetic factors affecting varying small portions of the connectome in different states. Except for the modality-static components, most of the remaining SNP components overall showed lower across-state similarity compared to dFNC. This is likely attributable to the differences in data structure. With genotypes being additively coded into numbers of minor alleles (i.e., 0, 1, and 2) and dFNC features being continuous, the highly discrete SNP data tends to present more sparse distributions in covariation with specific patterns, as evident by the higher average kurtosis compared to dFNC. In other words, the top and background SNPs were more disparate, only highly relevant SNPs were aggregated into the same component without as many intermediate relevant features as in the dFNC components. Consequently, when jointly analyzed with state-specific dFNC features in dynamic fusions, despite the same input SNPs, the covariation

patterns changed, and the top SNPs changed also, and showed lower overlap (i.e., similarity) across parallel fusions than dFNC due to its sparse nature.

A total of 53 out of 131 components across parallel fusions showed differences between SZ cases and controls and were validated as SZ-relevant components. These components were overall evenly distributed across the dynamism range, as shown in Table 1 and Figure 2, indicating no bias in high or low dynamism for SZ relevance. The most discriminating component is State3_jICA7, whose dFNC modality explained 8.18% of the variance in the case-control difference. Its connectogram is shown in Figure 3, combined with the labels of involved ICNs, highlighting a subset of the connectome which could described as thalamus and subthalamus/hypothalamus-seeded connections to other ICNs. State3_jICA7 was paired with State1_jICA9 as the most similar component across parallel fusions, the latter being the second top SZ-discriminating component (5.43% variance explained) whose dFNC modality also presented a similar thalamus and subthalamus/hypothalamus seeded connectivity pattern. It has been well acknowledged that the thalamus plays a key role in information processing, and the abnormalities in the frontal-thalamic-cerebellar circuitry is involved in a wide range of symptoms, including SZ[67,68]. Neuroimaging studies lend support for reduced gray matter in the thalamus of patients with SZ compared with controls[69,70]. Thalamic functional dysconnectivity has also been documented in SZ[71-73]. Our findings echo previous work to confirm disrupted thalamic connections in SZ, and further reveal a thalamus-seeded connectivity pattern that existed in multiple dynamic states, likely reflecting a primary composition of the connectome. The linked genomic factors of State1_jICA9 and State3_jICA7 shared 37% of the annotated genes, both enriched for regulation of cell projection organization, a biological process that results in the assembly, arrangement of constituent parts, or disassembly of a prolongation or process extending from a cell, e.g. a flagellum or axon, as defined by Gene Ontology. This raises the question of whether the disrupted cell projection organization may contribute to functional dysconnectivity, which requires the integration of multi-scale data resources to verify and understand how it happens. State1_jICA9 was also enriched for the regulation of synaptic plasticity, as well as learning

and memory. There has been the hypothesis of synaptic dysfunction in SZ[74,75]. Regional decrease in the density of postsynaptic elements has been reported for SZ in a meta-analysis of postmortem brain studies[76]. The current finding also finds support from previous work where reduced thalamic-prefrontal connectivity was associated with impaired working memory in SZ[72]. While in-depth functional annotation is beyond the scope of the current study, our observation encourages further investigations at the cellular level on how the identified genomic risk translates into functional dysconnectivity between the thalamus and other brain networks that are characteristic of SZ.

Another pair of SZ-relevant components with intermediate similarity included State1_jICA13 and State3_jICA5, both of which highlighted cerebellum-seeded connections to other ICNs (Figure 4), explaining 1.47% and 3.33% variances in case-control differences, respectively. Anatomical and functional alterations in the cerebellar region have been consistently reported in SZ[77-79]. Also as an important region of the frontal-thalamo-cerebellar circuitry, the role of the cerebellum in cognitive symptoms of SZ has been more and more emphasized [80-82]. More recently, gray matter reduction in the cerebellum has been suggested to modulate static and dynamic cerebellum dysconnections with the thalamus and frontal regions in SZ[83]. Our findings of the cerebellum seeded connectivity pattern, along with the thalamus seeded component discussed above, are in high concert with the literature to emphasize the key seed roles of these two regions in SZ-related dysconnectivity. The linked genomic factors of these two pairs shared 31% of the annotated genes, although enriched in different biological processes. It's noted that in addition to synapse organization whose relevance to SZ has been discussed above, State1_jICA13 was enriched for regulation of neuron projection development, which also plays an important role in the neuropathology of SZ. Neuron projection may refer to any process extending from a neural cell, such as axons or dendrites that are involved in communication between neurons and hence functional connectivity. Again, despite our observation that these enriched biological processes may be reasonably linked to the dFNC features, further verification is warranted and investigations are needed to

characterize whether genomic risk affects the brain through regulating gene expression or other mechanisms.

State1_jICA30 and State2_jICA32 are representative of modality-static components, where the SNP components were almost the same. The modality-static SNP components were in general super sparse with heavily weighed top SNPs that were more regional rather than distributed across the genome. The linked dFNC factors also involved a small portion of the connectome. Specifically for the highlighted pair, their SNP components highlighted the same annotated genes: *MFHAS1, MSRA, and SGK223* (Supplemental Table 1). The linked dFNC components reflected connections between visual, cognitive control, and default mode networks (Figure 5). It's noted that *SGK223* (also known as *PRAG1* or pragmin) induces Rho-dependent cell contraction in neuronal cells and may regulate neurite outgrowth[84]. It remains to be elucidated whether any additional pathways may bridge between the genes and dFNC features.

Last but not least, we have identified joint components located at the low end of across-state similarity, such as State1_jICA4 and State1_jICA6, as presented in Table 1 and Figure 6. Note that although these two components were validated as SZ-relevant, even their top paired components State4_jICA19 and State4_jICA14 (as shown in Table 1) did not show significant SZ-discrimination, which supports their uniqueness and echoes the notion that studying functional connectivity from a dynamic perspective promises an enriched view of disease-related abnormalities. The SNP modality of these two components showed even lower across-state similarity, indicating that these genomic factors could likely be elicited only upon fusion with dFNC. And we interpret them as time-varying SNP manifolds given the high level of dynamism.

The connectogram of State1_jICA4 presents an insula-seeded connectivity pattern while its SNP component was enriched for regulation of cell projection organization. It is interesting to note that State1_jICA1 and State1_jICA13 were enriched for the same biological process, despite the fact that they

were not correlated with one another. This observation indicated that the State1_jICA4 SNPs might be complementary to State1_jICA13 to provide a more complete picture of the genomic factor that confers risk to SZ by affecting cell projection organization. This presents the benefit of dynamic fusion to expand the SNP data for time-varying manifolds that may provide additional insights into the underlying biology. There has been plenty of evidence for the insula pathology in SZ[85], including decreased gray matter[69,70], and functional dysconnectivity that showed correlation with cognitive function and negative symptoms [86], as well as implicated in the SZ-related aberrant salience network connectivity during information processing[87]. State1_jICA6 described an association between MTG-seeded connections and a genomic factor enriched for the regulation of synaptic plasticity. Reduced gray matter has been documented for MTG in SZ[88]. Both structural abnormalities in MTG and MTG dysconnectivity have been linked to auditory verbal hallucinations in SZ[89,90]. The SNPs and genes identified in State1_jICA6 served as a complement to those of State1_jICA9 and State1_jICA13 to provide a more complete view of the synapse-related genomic risk for SZ. Given that synaptic plasticity has been suggested to underlie brain connectivity[91], it is reasonable that several of our identified SNP components were enriched for this biological process. While these SNP components did not significantly overlap, it is intriguing to look into whether the component-specific genes might show tissue or regional specificity to result in different linked genes of different dFNC components.

This work presents a novel approach and some initial evidence to showcase how dynamic SNP-dFNC fusion might expand the SNP modality for biologically meaningful time-varying manifolds that offer additional insights into SZ. The results should be interpreted in light of the following limitations. First, a more sophisticated adaptive normalization may be needed to better compensate for the difference in SNP and dFNC data structure so that more balanced data decomposition can be achieved to allow both modalities contributing equally to the components[92]. Second, fuzzy clustering or meta-state approaches may be employed to allow each dFNC time window to have a probabilistic rather than categorical state membership, or represent a linear combination of dynamic states, rather than being assigned to one

state[42,93]. This not only provides an enriched view of dFNC but also addresses the issue of missing values in state-average dFNC features due to some individuals never entering a specific state. Third, the current SNP-dFNC dynamic fusion utilized the population cohort of UKB for discovery given its large sample size. Although we validated the findings in an aggregated SZ cohort, it remains a question of whether a dynamic fusion directly applied to SZ cohorts may yield additional insights.

In conclusion, this work aims to present a novel dynamic fusion framework, to compare the dynamic or static nature of the decompositions across multiple data fusions. Overall, results support the hypothesis that dynamic fusion yields "static" and "time-varying" components for SNP and dFNC modalities. As expected, a subset of the SNP components was highly static, whereas another subset of the SNP components was dynamically varying. The time-varying SNP components uniquely elicited by the dynamic fusion complement other components in terms of biological interpretation. This dynamic fusion framework thus allows expanding the SNP modality to manifolds in the time dimension, which provides a unique lens to elicit unique SNP correlates otherwise unseen, promising additional insights on how genetic risk links to disease-related dysconnectivity.

ACKNOWLEDGEMENTS

This project was funded by the National Institutes of Health (P20GM103472, R01EB005846, 1R01EB006841, R01MH106655, 5R01MH094524) and the National Science Foundation (1539067).

COMPETING FINANCIAL INTERESTS

The authors declare no conflict of interest.

REFERENCES

1. Sullivan, P.F., Kendler, K.S., and Neale, M.C. (2003). Schizophrenia as a complex trait - Evidence from a meta-analysis of twin studies. Arch Gen Psychiat *60*, 1187-1192. DOI 10.1001/archpsyc.60.12.1187.
2. Glahn, D.C., Paus, T., and Thompson, P.M. (2007). Imaging genomics: Mapping the influence of genetics on brain structure and function. Human Brain Mapping *28*, 461-463. Doi 10.1002/Hbm.20416.
3. Anttila, V., Bulik-Sullivan, B., Finucane, H.K., Walters, R.K., Bras, J., Duncan, L., Escott-Price, V., Falcone, G.J., Gormley, P., Malik, R., et al. (2018). Analysis of shared heritability in common disorders of the brain. Science *360*, 1313-+. ARTN eaap8757 10.1126/science.aap8757.
4. Pettersson, E., Lichtenstein, P., Larsson, H., Song, J., Agrawal, A., Borglum, A.D., Bulik, C.M., Daly, M.J., Davis, L.K., Demontis, D., et al. (2019). Genetic influences on eight psychiatric disorders based on family data of 4 408 646 full and half-siblings, and genetic data of 333 748 cases and controls (vol 49, pg 351, 2019). Psychol Med *49*, 351-351. 10.1017/S0033291718002945.
5. Sandin, S., Lichtenstein, P., Kuja-Halkola, R., Hultman, C., Larsson, H., and Reichenberg, A. (2017). The Heritability of Autism Spectrum Disorder. Jama-J Am Med Assoc *318*, 1182-1184. 10.1001/jama.2017.12141.
6. Gatz, M., Reynolds, C.A., Fratiglioni, L., Johansson, B., Mortimer, J.A., Berg, S., Fiske, A., and Pedersen, N.L. (2006). Role of genes and environments for explaining Alzheimer disease. Arch Gen Psychiat *63*, 168-174. DOI 10.1001/archpsyc.63.2.168.
7. Sullivan, P.F., Agrawal, A., Bulik, C.M., Andreassen, O.A., Borglum, A.D., Breen, G., Cichon, S., Edenberg, H.J., Faraone, S.V., Gelernter, J., et al. (2018). Psychiatric Genomics: An Update and an Agenda. Am J Psychiat *175*, 15-27. 10.1176/appi.ajp.2017.17030283.
8. Pettersson, E., Lichtenstein, P., Larsson, H., Song, J., Agrawal, A., Børglum, A., Bulik, C., Daly, M., Davis, L., and Demontis, D. (2019). Genetic influences on eight psychiatric disorders based on family data of 4 408 646 full and half-siblings, and genetic data of 333 748 cases and controls. Psychol Med *49*, 1166-1173.
9. Lee, S.H., Ripke, S., Neale, B.M., Faraone, S.V., Purcell, S.M., Perlis, R.H., Mowry, B.J., Thapar, A., Goddard, M.E., Witte, J.S., et al. (2013). Genetic relationship between five psychiatric disorders estimated from genome-wide SNPs. Nat Genet *45*, 984-+. Doi 10.1038/Ng.2711.
10. Ashley, E.A. (2016). Towards precision medicine. Nat Rev Genet *17*, 507-522. 10.1038/nrg.2016.86.
11. Freudenberg-Hua, Y., Li, W.T., and Davies, P. (2018). The Role of Genetics in Advancing Precision Medicine for Alzheimer's Disease-A Narrative Review. Front Med-Lausanne *5*. ARTN 108 10.3389/fmed.2018.00108.
12. Gandal, M.J., Leppa, V., Won, H.J., Parikshak, N.N., and Geschwind, D.H. (2016). The road to precision psychiatry: translating genetics into disease mechanisms. Nat Neurosci *19*, 1397-1407. 10.1038/nn.4409.
13. Shen, L., and Thompson, P.M. (2020). Brain Imaging Genomics: Integrated Analysis and Machine Learning. P Ieee *108*, 125-162. 10.1109/Jproc.2019.2947272.
14. Insel, T., Cuthbert, B., Garvey, M., Heinssen, R., Pine, D.S., Quinn, K., Sanislow, C., and Wang, P. (2010). Research Domain Criteria (RDoC): Toward a New Classification Framework for Research on Mental Disorders. Am J Psychiat *167*, 748-751. 10.1176/appi.ajp.2010.09091379.
15. Cuthbert, B.N. (2014). The RDoC framework: facilitating transition from ICD/DSM to dimensional approaches that integrate neuroscience and psychopathology. World Psychiatry *13*, 28-35. 10.1002/wps.20087.

16. Cuthbert, B.N., and Insel, T.R. (2013). Toward the future of psychiatric diagnosis: the seven pillars of RDoC. BMC Med *11*, 126. 10.1186/1741-7015-11-126.
17. Insel, T.R. (2014). The NIMH Research Domain Criteria (RDoC) Project: Precision Medicine for Psychiatry. Am J Psychiat *171*, 395-397. 10.1176/appi.ajp.2014.14020138.
18. Insel, T.R., and Cuthbert, B.N. (2015). Brain disorders? Precisely. Science *348*, 499-500. 10.1126/science.aab2358.
19. Liu, J.Y., and Calhoun, V.D. (2014). A review of multivariate analyses in imaging genetics. Frontiers in Neuroinformatics *8*. Artn 29 10.3389/Fninf.2014.00029.
20. Liu, J.Y., Pearlson, G., Windemuth, A., Ruano, G., Perrone-Bizzozero, N.I., and Calhoun, V. (2009). Combining fMRI and SNP Data to Investigate Connections Between Brain Function and Genetics Using Parallel ICA. Human Brain Mapping *30*, 241-255. Doi 10.1002/Hbm.20508.
21. Chen, J., Calhoun, V.D., Pearlson, G.D., Perrone-Bizzozero, N., Sui, J., Turner, J.A., Bustillo, J.R., Ehrlich, S., Sponheim, S.R., Canive, J.M., et al. (2013). Guided exploration of genomic risk for gray matter abnormalities in schizophrenia using parallel independent component analysis with reference. Neuroimage *83C*, 384-396. 10.1016/j.neuroimage.2013.05.073.
22. Chi, E.C., Allen, G.I., Zhou, H., Kohannim, O., Lange, K., and Thompson, P.M. (2013). Imaging Genetics Via Sparse Canonical Correlation Analysis. 2013 Ieee 10th International Symposium on Biomedical Imaging (Isbi), 740-743.
23. Le Cao, K.A., Rossouw, D., Robert-Granie, C., and Besse, P. (2008). A Sparse PLS for Variable Selection when Integrating Omics Data. Statistical Applications in Genetics and Molecular Biology *7*.
24. Andrew, G., Arora, R., Bilmes, J., and Livescu, K. (2013). Deep canonical correlation analysis. (PMLR), pp. 1247-1255.
25. Benton, A., Khayrallah, H., Gujral, B., Reisinger, D.A., Zhang, S., and Arora, R. (2017). Deep generalized canonical correlation analysis. arXiv preprint arXiv:1702.02519.
26. Stahl, E.A., Breen, G., Forstner, A.J., McQuillin, A., Ripke, S., Trubetskoy, V., Mattheisen, M., Wang, Y., Coleman, J.R., and Gaspar, H.A. (2019). Genome-wide association study identifies 30 loci associated with bipolar disorder. Nat Genet *51*, 793-803.
27. Trubetskoy, V., Pardinas, A.F., Qi, T., Panagiotaropoulou, G., Awasthi, S., Bigdeli, T.B., Bryois, J., Chen, C.Y., Dennison, C.A., Hall, L.S., et al. (2022). Mapping genomic loci implicates genes and synaptic biology in schizophrenia. Nature *604*, 502-508. 10.1038/s41586-022-04434-5.
28. Howard, D.M., Adams, M.J., Clarke, T.K., Hafferty, J.D., Gibson, J., Shirali, M., Coleman, J.R.I., Hagenaars, S.P., Ward, J., Wigmore, E.M., et al. (2019). Genome-wide meta-analysis of depression identifies 102 independent variants and highlights the importance of the prefrontal brain regions. Nat Neurosci *22*, 343-+. 10.1038/s41593-018-0326-7.
29. Jansen, I.E., Savage, J.E., Watanabe, K., Bryois, J., Williams, D.M., Steinberg, S., Sealock, J., Karlsson, I.K., Hägg, S., Athanasiu, L., et al. (2020). Genome-wide meta-analysis identifies new loci and functional pathways influencing Alzheimer's disease risk (vol 51, 404, 2019). Nat Genet *52*, 354-354. 10.1038/s41588-019-0573-x.
30. Kauppi, K., Westlye, L.T., Tesli, M., Bettella, F., Brandt, C.L., Mattingsdal, M., Ueland, T., Espeseth, T., Agartz, I., Melle, I., et al. (2015). Polygenic Risk for Schizophrenia Associated With Working Memory-related Prefrontal Brain Activation in Patients With Schizophrenia and Healthy Controls. Schizophrenia Bull *41*, 736-743. 10.1093/schbul/sbu152.
31. Chen, J., Calhoun, V.D., Lin, D., Perrone-Bizzozero, N.I., Bustillo, J.R., Pearlson, G.D., Potkin, S.G., van Erp, T.G.M., Macciardi, F., Ehrlich, S., et al. (2019). Shared Genetic Risk of Schizophrenia and Gray Matter Reduction in 6p22.1. Schizophr Bull *45*, 222-232. 10.1093/schbul/sby010.
32. Miller, J.A., Scult, M.A., Conley, E.D., Chen, Q., Weinberger, D.R., and Hariri, A.R. (2018). Effects of Schizophrenia Polygenic Risk Scores on Brain Activity and Performance During Working Memory Subprocesses in Healthy Young Adults. Schizophrenia Bull *44*, 844-853. 10.1093/schbul/sbx140.

33. Grama, S., Willcocks, I., Hubert, J.J., Pardinas, A.F., Legge, S.E., Bracher-Smith, M., Menzies, G.E., Hall, L.S., Pocklington, A.J., Anney, R.J.L., et al. (2020). Polygenic risk for schizophrenia and subcortical brain anatomy in the UK Biobank cohort. Transl Psychiatry *10*, 309. 10.1038/s41398-020-00940-0.
34. Zhu, X., Ward, J., Cullen, B., Lyall, D.M., Strawbridge, R.J., Smith, D.J., and Lyall, L.M. (2021). Polygenic risk for schizophrenia, brain structure, and environmental risk in UK biobank. Schizophrenia Bulletin Open *2*, sgab042.
35. Dimitriadis, S.I., Lancaster, T.M., Perry, G., Tansey, K.E., Jones, D.K., Singh, K.D., Zammit, S., Smith, G.D., Hall, J., O'Donovan, M.C., et al. (2021). Global Brain Flexibility During Working Memory Is Reduced in a High-Genetic-Risk Group for Schizophrenia. Biol Psychiat-Cogn N *6*, 1176-1184. 10.1016/j.bpsc.2021.01.007.
36. Allen, E.A., Damaraju, E., Plis, S.M., Erhardt, E.B., Eichele, T., and Calhoun, V.D. (2014). Tracking Whole-Brain Connectivity Dynamics in the Resting State. Cerebral Cortex *24*, 663-676. 10.1093/cercor/bhs352.
37. Calhoun, V.D., Miller, R., Pearlson, G., and Adali, T. (2014). The Chronnectome: Time-Varying Connectivity Networks as the Next Frontier in fMRI Data Discovery. Neuron *84*, 262-274. 10.1016/j.neuron.2014.10.015.
38. Damaraju, E., Allen, E.A., Belger, A., Ford, J.M., McEwen, S., Mathalon, D.H., Mueller, B.A., Pearlson, G.D., Potkin, S.G., Preda, A., et al. (2014). Dynamic functional connectivity analysis reveals transient states of dysconnectivity in schizophrenia. Neuroimage-Clin *5*, 298-308. 10.1016/j.nicl.2014.07.003.
39. Iraji, A., Faghiri, A., Lewis, N., Fu, Z.N., Rachakonda, S., and Calhoun, V.D. (2021). Tools of the trade: estimating time-varying connectivity patterns from fMRI data. Soc Cogn Affect Neur *16*, 849-874. 10.1093/scan/nsaa114.
40. Abrol, A., Damaraju, E., Miller, R.L., Stephen, J.M., Claus, E.D., Mayer, A.R., and Calhoun, V.D. (2017). Replicability of time-varying connectivity patterns in large resting state fMRI samples. Neuroimage *163*, 160-176. 10.1016/j.neuroimage.2017.09.020.
41. Miller, R.L., Abrol, A., Adali, T., Levin-Schwarz, Y., and Calhoun, V.D. (2018). Resting-State fMRI Dynamics and Null Models: Perspectives, Sampling Variability, and Simulations. Front Neurosci-Switz *12*. ARTN 551 10.3389/fnins.2018.00551.
42. Miller, R.L., Yaesoubi, M., Turner, J.A., Mathalon, D., Preda, A., Pearlson, G., Adali, T., and Calhoun, V.D. (2016). Higher Dimensional Meta-State Analysis Reveals Reduced Resting fMRI Connectivity Dynamism in Schizophrenia Patients. Plos One *11*. ARTN e0149849 10.1371/journal.pone.0149849.
43. Rashid, B., Arbabshirani, M.R., Damaraju, E., Cetin, M.S., Miller, R., Pearlson, G.D., and Calhoun, V.D. (2016). Classification of schizophrenia and bipolar patients using static and dynamic resting-state fMRI brain connectivity. Neuroimage *134*, 645-657. 10.1016/j.neuroimage.2016.04.051.
44. Rabany, L., Brocke, S., Calhoun, V.D., Pittman, B., Corbera, S., Wexler, B.E., Bell, M.D., Pelphrey, K., Pearlson, G.D., and Assaf, M. (2019). Dynamic functional connectivity in schizophrenia and autism spectrum disorder: Convergence, divergence and classification (vol 24, 101966, 2019). Neuroimage-Clin *24*. ARTN 102012 10.1016/j.nicl.2019.102012.
45. Vergara, V.M., Mayer, A.R., Kiehl, K.A., and Calhoun, V.D. (2018). Dynamic functional network connectivity discriminates mild traumatic brain injury through machine learning. Neuroimage-Clin *19*, 30-37. 10.1016/j.nicl.2018.03.017.
46. Elliott, L.T., Sharp, K., Alfaro-Almagro, F., Shi, S.N., Miller, K.L., Douaud, G., Marchini, J., and Smith, S.M. (2018). Genome-wide association studies of brain imaging phenotypes in UK Biobank. Nature *562*, 210-+. 10.1038/s41586-018-0571-7.
47. Rashid, B., Chen, J., Rashid, I., Damaraju, E., Liu, J., Miller, R., Agcaoglu, O., van Erp, T.G.M., Lim, K.O., Turner, J.A., et al. (2019). A framework for linking resting-state

chronnectome/genome features in schizophrenia: A pilot study. Neuroimage *184*, 843-854. 10.1016/j.neuroimage.2018.10.004.

48. Du, Y., Fu, Z., Sui, J., Gao, S., Xing, Y., Lin, D., Salman, M., Abrol, A., Rahaman, M.A., and Chen, J. (2020). NeuroMark: An automated and adaptive ICA based pipeline to identify reproducible fMRI markers of brain disorders. NeuroImage: Clinical *28*, 102375.
49. Aine, C.J., Bockholt, H.J., Bustillo, J.R., Canive, J.M., Caprihan, A., Gasparovic, C., Hanlon, F.M., Houck, J.M., Jung, R.E., Lauriello, J., et al. (2017). Multimodal Neuroimaging in Schizophrenia: Description and Dissemination. Neuroinformatics *15*, 343-364. 10.1007/s12021-017-9338-9.
50. Tamminga, C.A., Ivleva, E.I., Keshavan, M.S., Pearlson, G.D., Clementz, B.A., Witte, B., Morris, D.W., Bishop, J., Thaker, G.K., and Sweeney, J.A. (2013). Clinical Phenotypes of Psychosis in the Bipolar-Schizophrenia Network on Intermediate Phenotypes (B-SNIP). Am J Psychiat *170*, 1263-1274. 10.1176/appi.ajp.2013.12101339.
51. Kochunov, P., Coyle, T.R., Rowland, L.M., Jahanshad, N., Thompson, P.M., Kelly, S., Du, X.M., Sampath, H., Bruce, H., Chiappelli, J., et al. (2017). Association of White Matter With Core Cognitive Deficits in Patients With Schizophrenia. Jama Psychiatry *74*, 958-966. 10.1001/jamapsychiatry.2017.2228.
52. Yu, Q.B., Erhardt, E.B., Sui, J., Du, Y.H., He, H., Hjelm, D., Cetin, M.S., Rachakonda, S., Miller, R.L., Pearlson, G., and Calhoun, V.D. (2015). Assessing dynamic brain graphs of time-varying connectivity in fMRI data: Application to healthy controls and patients with schizophrenia. Neuroimage *107*, 345-355. 10.1016/j.neuroimage.2014.12.020.
53. Chen, J., Rashid, B., Yu, Q., Liu, J., Lin, D., Du, Y., Sui, J., and Calhoun, V.D. (2018). Variability in Resting State Network and Functional Network Connectivity Associated With Schizophrenia Genetic Risk: A Pilot Study. Front Neurosci *12*, 114. 10.3389/fnins.2018.00114.
54. Skatun, K.C., Kaufmann, T., Brandt, C.L., Doan, N.T., Alnaes, D., Tonnesen, S., Biele, G., Vaskinn, A., Melle, I., Agartz, I., et al. (2018). Thalamo-cortical functional connectivity in schizophrenia and bipolar disorder. Brain Imaging and Behavior *12*, 640-652. 10.1007/s11682-017-9714-y.
55. Bycroft, C., Freeman, C., Petkova, D., Band, G., Elliott, L.T., Sharp, K., Motyer, A., Vukcevic, D., Delaneau, O., and O'Connell, J. (2018). The UK Biobank resource with deep phenotyping and genomic data. Nature *562*, 203-209.
56. O'Connell, J., Sharp, K., Shrine, N., Wain, L., Hall, I., Tobin, M., Zagury, J.-F., Delaneau, O., and Marchini, J. (2016). Haplotype estimation for biobank-scale data sets. Nat Genet *48*, 817-820.
57. A reference panel of 64,976 haplotypes for genotype imputation. (2016). Nat Genet *48*, 1279-1283.
58. Huang, J., Howie, B., McCarthy, S., Memari, Y., Walter, K., Min, J.L., Danecek, P., Malerba, G., Trabetti, E., and Zheng, H.-F. (2015). Improved imputation of low-frequency and rare variants using the UK10K haplotype reference panel. Nat Commun *6*, 8111.
59. Choi, S.W., Mak, T.S.-H., and O'Reilly, P.F. (2020). Tutorial: a guide to performing polygenic risk score analyses. Nature protocols *15*, 2759-2772.
60. Purcell, S., Neale, B., Todd-Brown, K., Thomas, L., Ferreira, M.A.R., Bender, D., Maller, J., Sklar, P., de Bakker, P.I.W., Daly, M.J., and Sham, P.C. (2007). PLINK: A tool set for whole-genome association and population-based linkage analyses. American Journal of Human Genetics *81*, 559-575. Doi 10.1086/519795.
61. Littlejohns, T.J., Holliday, J., Gibson, L.M., Garratt, S., Oesingmann, N., Alfaro-Almagro, F., Bell, J.D., Boultwood, C., Collins, R., and Conroy, M.C. (2020). The UK Biobank imaging enhancement of 100,000 participants: rationale, data collection, management and future directions. Nat Commun *11*, 2624.

62. Fu, Z., Iraji, A., Turner, J.A., Sui, J., Miller, R., Pearlson, G.D., and Calhoun, V.D. (2021). Dynamic state with covarying brain activity-connectivity: On the pathophysiology of schizophrenia. Neuroimage *224*, 117385.
63. Du, Y.H., and Fan, Y. (2013). Group information guided ICA for fMRI data analysis. Neuroimage *69*, 157-197. 10.1016/j.neuroimage.2012.11.008.
64. Calhoun, V., Silva, R., and Liu, J. (2007). Identification of multimodal MRI and EEG biomarkers using joint-ICA and divergence criteria. (IEEE), pp. 151-156.
65. Bell, A.J., and Sejnowski, T.J. (1995). An information-maximization approach to blind separation and blind deconvolution. Neural Comput *7*, 1129-1159.
66. Thomas, P.D., Ebert, D., Muruganujan, A., Mushayahama, T., Albou, L.P., and Mi, H. (2022). PANTHER: Making genome - scale phylogenetics accessible to all. Protein Science *31*, 8-22.
67. Andreasen, N.C. (1997). The role of the thalamus in schizophrenia. Can J Psychiat *42*, 27-33. Doi 10.1177/070674379704200104.
68. Pergola, G., Selvaggi, P., Trizio, S., Bertolino, A., and Blasi, G. (2015). The role of the thalamus in schizophrenia from a neuroimaging perspective. Neuroscience & Biobehavioral Reviews *54*, 57-75.
69. Fornito, A., Yücel, M., Patti, J., Wood, S.J., and Pantelis, C. (2009). Mapping grey matter reductions in schizophrenia: an anatomical likelihood estimation analysis of voxel-based morphometry studies. Schizophrenia research *108*, 104-113.
70. Glahn, D.C., Laird, A.R., Ellison-Wright, I., Thelen, S.M., Robinson, J.L., Lancaster, J.L., Bullmore, E., and Fox, P.T. (2008). Meta-analysis of gray matter anomalies in schizophrenia: application of anatomic likelihood estimation and network analysis. Biological psychiatry *64*, 774-781.
71. Gong, J., Luo, C., Li, X., Jiang, S., Khundrakpam, B.S., Duan, M., Chen, X., and Yao, D. (2019). Evaluation of functional connectivity in subdivisions of the thalamus in schizophrenia. The British Journal of Psychiatry *214*, 288-296.
72. Giraldo-Chica, M., Rogers, B.P., Damon, S.M., Landman, B.A., and Woodward, N.D. (2018). Prefrontal-thalamic anatomical connectivity and executive cognitive function in schizophrenia. Biological psychiatry *83*, 509-517.
73. Ferri, J., Ford, J., Roach, B., Turner, J., Van Erp, T., Voyvodic, J., Preda, A., Belger, A., Bustillo, J., and O'Leary, D. (2018). Resting-state thalamic dysconnectivity in schizophrenia and relationships with symptoms. Psychol Med *48*, 2492-2499.
74. Frankle, W.G., Lerma, J., and Laruelle, M. (2003). The synaptic hypothesis of schizophrenia. Neuron *39*, 205-216.
75. Stephan, K.E., Baldeweg, T., and Friston, K.J. (2006). Synaptic plasticity and dysconnection in schizophrenia. Biological psychiatry *59*, 929-939.
76. Berdenis van Berlekom, A., Muflihah, C.H., Snijders, G.J., MacGillavry, H.D., Middeldorp, J., Hol, E.M., Kahn, R.S., and De Witte, L.D. (2020). Synapse pathology in schizophrenia: a meta-analysis of postsynaptic elements in postmortem brain studies. Schizophrenia Bull *46*, 374-386.
77. Picard, H., Amado, I., Mouchet-Mages, S., Olié, J.-P., and Krebs, M.-O. (2008). The role of the cerebellum in schizophrenia: an update of clinical, cognitive, and functional evidences. Schizophrenia Bull *34*, 155-172.
78. Andreasen, N.C., and Pierson, R. (2008). The role of the cerebellum in schizophrenia. Biological psychiatry *64*, 81-88.
79. Rasser, P.E., Schall, U., Peck, G., Cohen, M., Johnston, P., Khoo, K., Carr, V.J., Ward, P.B., and Thompson, P.M. (2010). Cerebellar grey matter deficits in first-episode schizophrenia mapped using cortical pattern matching. Neuroimage *53*, 1175-1180.
80. Andreasen, N.C., O'Leary, D.S., Cizadlo, T., Arndt, S., Rezai, K., Ponto, L., Watkins, G.L., and Hichwa, R.D. (1996). Schizophrenia and cognitive dysmetria: a positron-emission tomography study of dysfunctional prefrontal-thalamic-cerebellar circuitry. Proceedings of the National Academy of Sciences *93*, 9985-9990.

81. Ide, J.S., and Chiang-shan, R.L. (2011). A cerebellar thalamic cortical circuit for error-related cognitive control. Neuroimage *54*, 455-464.
82. Schmahmann, J.D., Guell, X., Stoodley, C.J., and Halko, M.A. (2019). The theory and neuroscience of cerebellar cognition. Annual review of neuroscience *42*, 337-364.
83. He, H., Luo, C., Luo, Y., Duan, M., Yi, Q., Biswal, B.B., and Yao, D. (2019). Reduction in gray matter of cerebellum in schizophrenia and its influence on static and dynamic connectivity. Human brain mapping *40*, 517-528.
84. Tanaka, H., Katoh, H., and Negishi, M. (2006). Pragmin, a novel effector of Rnd2 GTPase, stimulates RhoA activity. Journal of Biological Chemistry *281*, 10355-10364.
85. Wylie, K.P., and Tregellas, J.R. (2010). The role of the insula in schizophrenia. Schizophrenia research *123*, 93-104.
86. Sheffield, J.M., Rogers, B.P., Blackford, J.U., Heckers, S., and Woodward, N.D. (2020). Insula functional connectivity in schizophrenia. Schizophrenia research *220*, 69-77.
87. White, T.P., Joseph, V., Francis, S.T., and Liddle, P.F. (2010). Aberrant salience network (bilateral insula and anterior cingulate cortex) connectivity during information processing in schizophrenia. Schizophrenia research *123*, 105-115.
88. Onitsuka, T., Shenton, M.E., Salisbury, D.F., Dickey, C.C., Kasai, K., Toner, S.K., Frumin, M., Kikinis, R., Jolesz, F.A., and McCarley, R.W. (2004). Middle and inferior temporal gyrus gray matter volume abnormalities in chronic schizophrenia: an MRI study. Am J Psychiat *161*, 1603-1611.
89. Cui, Y., Liu, B., Song, M., Lipnicki, D., Li, J., Xie, S., Chen, Y., Li, P., Lu, L., and Lv, L. (2018). Auditory verbal hallucinations are related to cortical thinning in the left middle temporal gyrus of patients with schizophrenia. Psychol Med *48*, 115-122.
90. Zhang, L., Li, B., Wang, H., Li, L., Liao, Q., Liu, Y., Bao, X., Liu, W., Yin, H., and Lu, H. (2017). Decreased middle temporal gyrus connectivity in the language network in schizophrenia patients with auditory verbal hallucinations. Neuroscience letters *653*, 177-182.
91. Stampanoni Bassi, M., Iezzi, E., Gilio, L., Centonze, D., and Buttari, F. (2019). Synaptic plasticity shapes brain connectivity: implications for network topology. International journal of molecular sciences *20*, 6193.
92. Khalilullah, K.I., Agcaoglu, O., Sui, J., Adali, T., Duda, M., and Calhoun, V.D. (2023). Multimodal fusion of multiple rest fMRI networks and MRI gray matter via parallel multilink joint ICA reveals highly significant function/structure coupling in Alzheimer's disease. Human Brain Mapping *44*, 5167-5179.
93. Ellis, C.A., Miller, R.L., and Calhoun, V.D. (2023). A Novel Explainable Fuzzy Clustering Approach for fMRI Dynamic Functional Network Connectivity Analysis. bioRxiv.

TABLES

Table 1: Summary of SZ-relevant SNP-dFNC components

State	Comp	r^2	p	FDR q	State_pair	Comp_pair	SNP similarity	dFNC similarity
1	2	0.86%	3.02E-03	1.03E-02	3	22	0.06	0.57
1	3	1.41%	1.48E-04	9.04E-04	4	23	0.26	0.47
1	4	1.32%	2.37E-04	1.27E-03	4	19	0.09	0.49
1	6	0.63%	1.15E-02	3.11E-02	4	14	0.07	0.39
1	9	5.34%	8.24E-14	3.84E-12	3	7	0.33	0.67
1	10	1.19%	4.89E-04	2.21E-03	4	29	0.15	0.67
1	12	1.26%	3.36E-04	1.57E-03	3	18	0.31	0.78
1	13	1.47%	1.06E-04	7.09E-04	3	5	0.35	0.78
1	16	1.43%	1.33E-04	8.47E-04	4	17	0.08	0.41
1	19	1.61%	4.98E-05	3.67E-04	2	2	0.42	0.62
1	29	0.90%	2.48E-03	8.90E-03	2	29	0.98	0.19
1	30	1.35%	2.08E-04	1.16E-03	2	32	1.00	0.57
1	33	0.57%	1.58E-02	3.97E-02	2	33	0.99	0.35
2	2	0.71%	3.55E-03	1.16E-02	1	19	0.42	0.62
2	4	0.57%	8.90E-03	2.49E-02	1	7	0.21	0.49
2	5	1.11%	2.60E-04	1.35E-03	4	20	0.15	0.63
2	8	0.46%	1.87E-02	4.43E-02	4	22	0.16	0.64
2	9	2.99%	1.72E-09	6.01E-08	1	18	0.25	0.60
2	12	1.17%	1.71E-04	9.98E-04	1	14	0.18	0.50
2	22	4.60%	6.21E-14	3.84E-12	4	15	0.43	0.86
2	25	1.95%	1.24E-06	1.45E-05	1	20	0.33	0.80
2	27	0.62%	6.56E-03	2.00E-02	1	15	0.56	0.81
2	28	0.58%	8.43E-03	2.46E-02	4	13	0.17	0.61
2	29	0.51%	1.31E-02	3.47E-02	1	29	0.98	0.19
2	30	1.09%	2.97E-04	1.44E-03	1	27	0.98	0.23
2	31	1.42%	3.61E-05	2.81E-04	1	34	0.99	0.33
2	32	2.91%	2.84E-09	7.95E-08	1	30	1.00	0.57
2	35	1.10%	2.80E-04	1.40E-03	1	35	1.00	0.30
3	2	2.95%	9.25E-08	1.62E-06	4	5	0.98	0.76
3	3	1.21%	6.79E-04	2.88E-03	4	9	0.13	0.60
3	4	1.88%	2.16E-05	1.78E-04	4	14	0.08	0.52
3	5	3.33%	1.40E-08	3.26E-07	1	13	0.35	0.78
3	7	8.18%	2.06E-19	2.88E-17	1	9	0.33	0.67
3	8	2.11%	6.76E-06	6.31E-05	2	11	0.25	0.60
3	9	2.31%	2.37E-06	2.56E-05	4	2	0.02	0.59
3	11	1.23%	5.93E-04	2.60E-03	4	12	0.15	0.60
3	15	2.68%	3.71E-07	5.19E-06	4	18	0.07	0.66
3	17	0.86%	4.17E-03	1.33E-02	4	23	0.26	0.55
3	21	1.06%	1.44E-03	5.61E-03	1	22	0.15	0.76
3	22	2.99%	7.61E-08	1.52E-06	1	2	0.06	0.57

3	23	0.98%	2.25E-03	8.28E-03	4	13	0.03	0.56
3	24	2.72%	2.97E-07	4.62E-06	1	8	0.18	0.56
3	28	0.61%	1.59E-02	3.97E-02	1	31	0.90	0.18
3	30	0.93%	2.82E-03	9.86E-03	2	32	0.99	0.34
3	31	0.59%	1.78E-02	4.29E-02	2	30	0.94	0.13
4	2	1.94%	8.86E-05	6.20E-04	3	9	0.02	0.59
4	9	0.76%	1.42E-02	3.69E-02	3	3	0.13	0.60
4	15	2.58%	5.96E-06	5.96E-05	2	22	0.43	0.86
4	18	0.90%	7.70E-03	2.29E-02	3	15	0.07	0.66
4	23	1.08%	3.56E-03	1.16E-02	3	17	0.26	0.55
4	30	0.72%	1.73E-02	4.25E-02	1	29	0.96	0.15
4	31	1.20%	2.12E-03	8.01E-03	2	33	0.97	0.15
4	35	0.87%	8.71E-03	2.49E-02	2	35	0.99	0.28

Table 2: Summary of enriched biological processes identified from SZ-relevant SNP-dFNC components.

State	Indcomp	GO pathway	Fold	FDR q
1	3	regulation of signaling (GO:0023051)	2.29	2.02E-02
		negative regulation of locomotion (GO:0040013)	6.45	3.31E-02
		neurogenesis (GO:0022008)	3.31	3.39E-02
		positive regulation of cell projection organization (GO:0031346)	6.84	3.80E-02
		neuron development (GO:0048666)	3.94	3.83E-02
1	**4**	**positive regulation of cell projection organization (GO:0031346)**	**8.65**	**1.08E-03**
1	**6**	**neurogenesis (GO:0022008)**	**3.91**	**1.92E-03**
		regulation of synaptic plasticity (GO:0048167)	**9.63**	**1.96E-02**
1	**9**	**positive regulation of cell projection organization (GO:0031346)**	**7.11**	**4.14E-03**
		regulation of synaptic plasticity (GO:0048167)	**10.45**	**4.43E-03**
		learning (GO:0007612)	**10.27**	**1.59E-02**
		memory (GO:0007613)	**10.9**	**4.70E-02**
1	12	positive regulation of cell projection organization (GO:0031346)	8.89	8.05E-04
		enzyme-linked receptor protein signaling pathway (GO:0007167)	5.37	4.06E-03
		anatomical structure morphogenesis (GO:0009653)	2.94	4.15E-03
		taxis (GO:0042330)	6.02	4.37E-03
		locomotion (GO:0040011)	5.8	4.45E-03
		multicellular organism development (GO:0007275)	2.31	4.60E-03
		chemotaxis (GO:0006935)	6.04	4.82E-03
		regulation of neuron projection development (GO:0010975)	6.36	5.05E-03
		axon guidance (GO:0007411)	8.56	1.61E-02
		ephrin receptor signaling pathway (GO:0048013)	22.88	2.16E-02
		regulation of calcium ion transport (GO:0051924)	7.61	2.30E-02
		neurogenesis (GO:0022008)	3.25	2.35E-02
1	**13**	**positive regulation of molecular function (GO:0044093)**	**3.19**	**1.60E-02**
		synapse organization (GO:0050808)	**7.28**	**2.23E-02**
		regulation of neuron projection development (GO:0010975)	**5.38**	**2.95E-02**
		regulation of calcium ion transport (GO:0051924)	**7.37**	**3.07E-02**
1	29	general adaptation syndrome (GO:0051866)	> 100	2.15E-02
2	2	regulation of intracellular signal transduction (GO:1902531)	3.21	2.15E-03
		learning or memory (GO:0007611)	7.94	3.65E-03
		positive regulation of cell projection organization (GO:0031346)	5.63	3.24E-02
		cardiac muscle cell contraction (GO:0086003)	20.6	4.16E-02
		regulation of long-term synaptic depression (GO:1900452)	41.52	4.49E-02
2	5	organic substance transport (GO:0071702)	2.78	7.51E-03
		establishment of localization (GO:0051234)	2.17	8.82E-03
		regulation of monoatomic ion transport (GO:0043269)	4.82	2.46E-02
2	9	calcium ion import (GO:0070509)	60.21	1.82E-02
2	22	positive regulation of cell projection organization (GO:0031346)	6.92	3.41E-02
2	25	regulation of trans-synaptic signaling (GO:0099177)	6.44	3.08E-03
		regulation of calcium ion transmembrane transport (GO:1903169)	11.33	3.68E-03
		learning (GO:0007612)	10.03	3.34E-02
		cardiac muscle cell action potential (GO:0086001)	21.72	3.61E-02
2	27	regulation of lyase activity (GO:0051339)	17.65	3.34E-02
		regulation of cell projection organization (GO:0031344)	4.64	3.41E-02
		positive regulation of collateral sprouting (GO:0048672)	69.33	3.97E-02
		positive regulation of axonogenesis (GO:0050772)	16.3	4.13E-02
		synapse organization (GO:0050808)	6.87	5.94E-02
3	1	regulation of voltage-gated calcium channel activity (GO:1901385)	> 100	3.99E-02
3	2	regulation of cell projection organization (GO:0031344)	5.15	2.81E-02
3	4	regulation of trans-synaptic signaling (GO:0099177)	6.32	3.28E-02
		modulation of chemical synaptic transmission (GO:0050804)	6.34	6.45E-02

3	**5**	**negative regulation of lyase activity (GO:0051350)**	**41.18**	**2.37E-02**
3	**7**	**cell-cell signaling (GO:0007267)**	**3.97**	**1.66E-02**
		system development (GO:0048731)	**2.37**	**2.68E-02**
		positive regulation of cell projection organization (GO:0031346)	**6.89**	**2.83E-02**
		multicellular organism development (GO:0007275)	**2.19**	**2.95E-02**
3	8	regulation of cell projection organization (GO:0031344)	5.17	1.75E-03
		calcium ion transmembrane transport (GO:0070588)	8.42	2.46E-02
3	9	regulation of synaptic plasticity (GO:0048167)	10.6	2.06E-02
		regulation of neuron projection development (GO:0010975)	5.97	4.70E-02
		regulation of heart rate by cardiac conduction (GO:0086091)	29.12	4.75E-02
3	15	action potential (GO:0001508)	18.16	2.83E-03
		cardiac muscle cell contraction (GO:0086003)	29.56	6.33E-03
		regulation of calcium ion transport (GO:0051924)	7.73	1.91E-02
3	17	cell projection organization (GO:0030030)	3.83	1.76E-03
		locomotion (GO:0040011)	5.63	2.07E-03
		neuron development (GO:0048666)	4.43	2.33E-03
		positive regulation of neurogenesis (GO:0050769)	8.47	5.29E-03
		regulation of long-term synaptic depression (GO:1900452)	47.67	1.89E-02
3	21	regulation of trans-synaptic signaling (GO:0099177)	5.83	2.53E-02
		regulation of adenylate cyclase activity (GO:0045761)	21.45	2.73E-02
		regulation of synaptic plasticity (GO:0048167)	9.15	3.15E-02
		glutamate receptor signaling pathway (GO:0007215)	22.88	3.75E-02
		calcium ion transmembrane transport (GO:0070588)	8.38	3.80E-02
3	22	cell-cell signaling (GO:0007267)	3.96	1.69E-02
		calcium ion transmembrane transport (GO:0070588)	9.46	2.05E-02
		atrial cardiac muscle cell action potential (GO:0086014)	54.48	4.20E-02
3	24	regulation of cell projection organization (GO:0031344)	4.43	1.92E-02
		anatomical structure morphogenesis (GO:0009653)	2.32	4.94E-02
		regulation of calcium-mediated signaling (GO:0050848)	12.68	5.01E-02
		learning or memory (GO:0007611)	5.96	5.04E-02
		regulation of neuron projection development (GO:0010975)	4.62	5.27E-02
4	18	regulation of cell communication (GO:0010646)	2.25	9.98E-03
		localization (GO:0051179)	1.95	1.95E-02
		actin filament-based movement (GO:0030048)	13.84	2.08E-02
		regulation of neuron projection development (GO:0010975)	4.87	4.18E-02

FIGURES

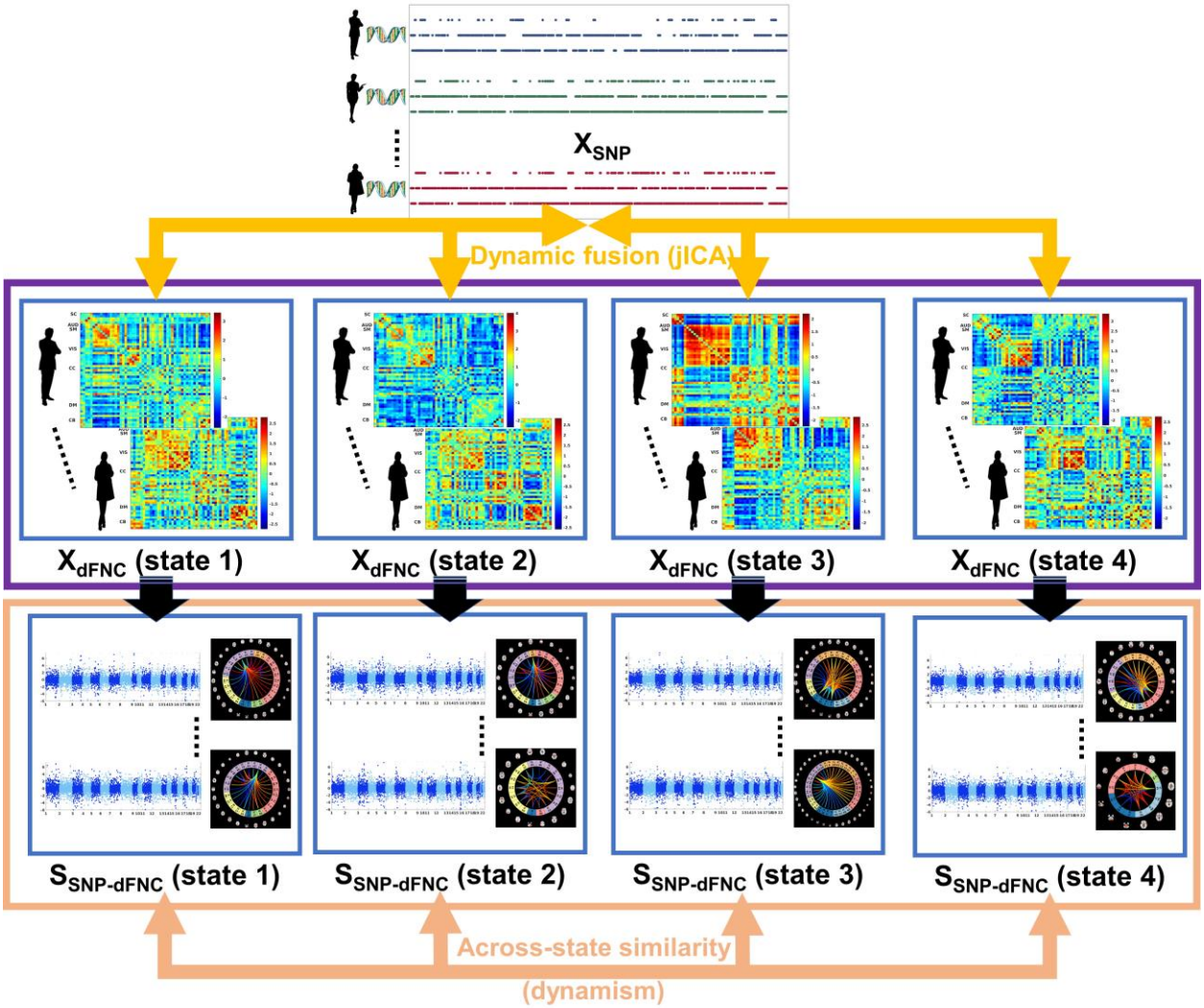

Figure 1: A diagram of dynamic fusion and estimation of across-state component similarity (dynamism). The SNP data X_{SNP} was fused with the dFNC features of each state, e.g., X_{dFNC} (state1), in parallel. $S_{SNP\text{-}dFNC}$ denotes the joint SNP-dFNC components yielded by the dynamic fusion. Across-state similarity was assessed between the four sets of components of state1-state4, to indicate dynamism, for SNP and dFNC modalities, respectively.

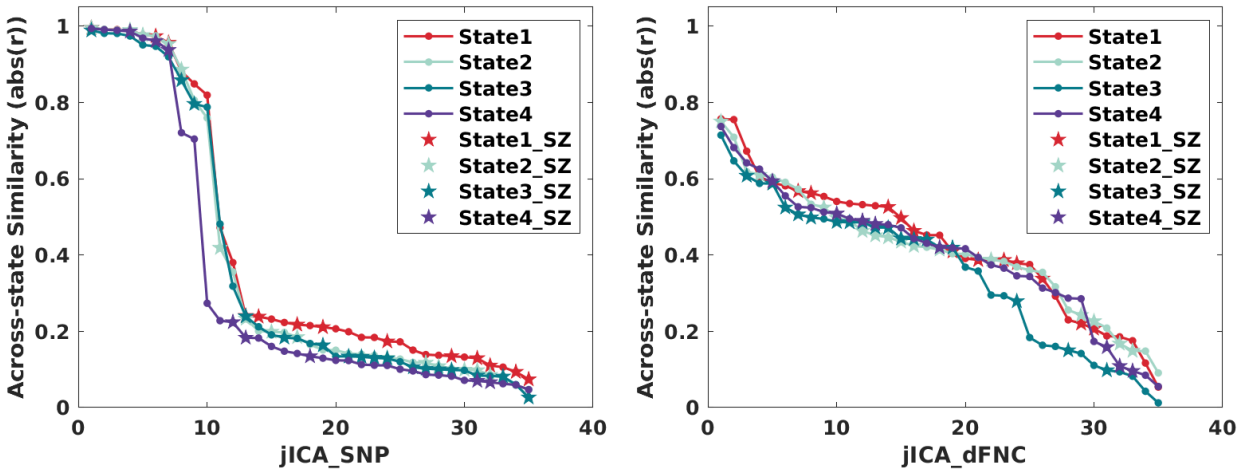

Figure 2: Plots of across-state similarity for SNP and dFNC, with asterisks highlighting SZ-related components.

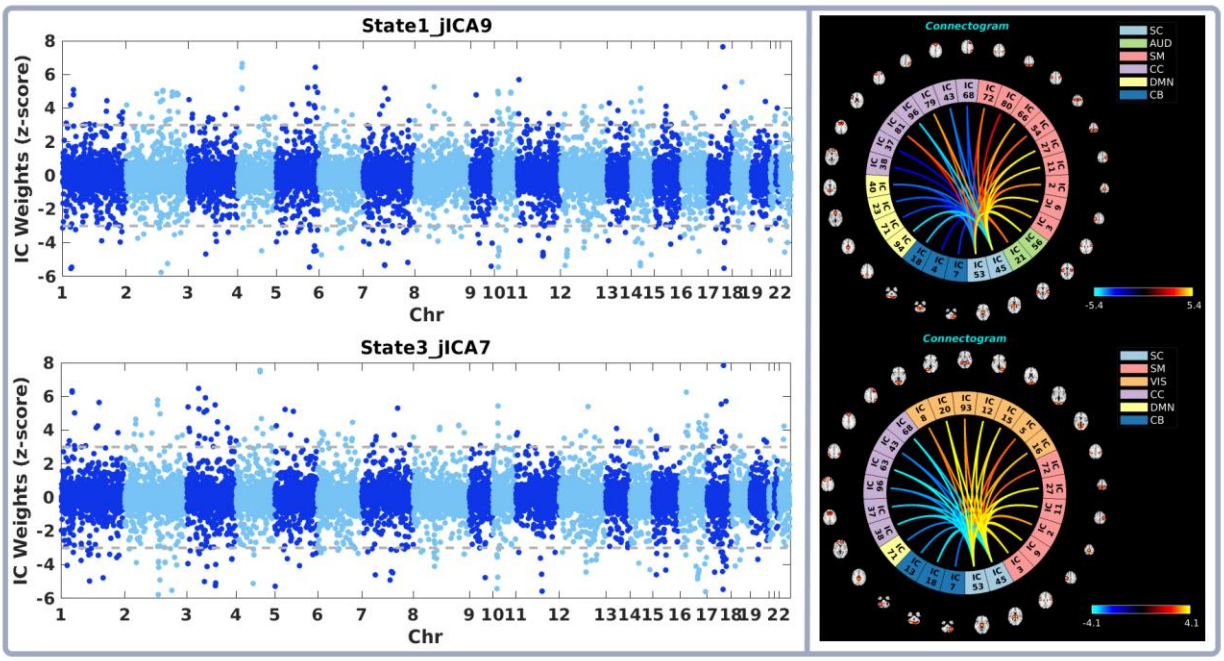

Figure 3: Manhattan and connectogram plots for State1_jICA9 (upper) and State3_jICA7 (lower), where dashed lines indicate |z-score| > 3.

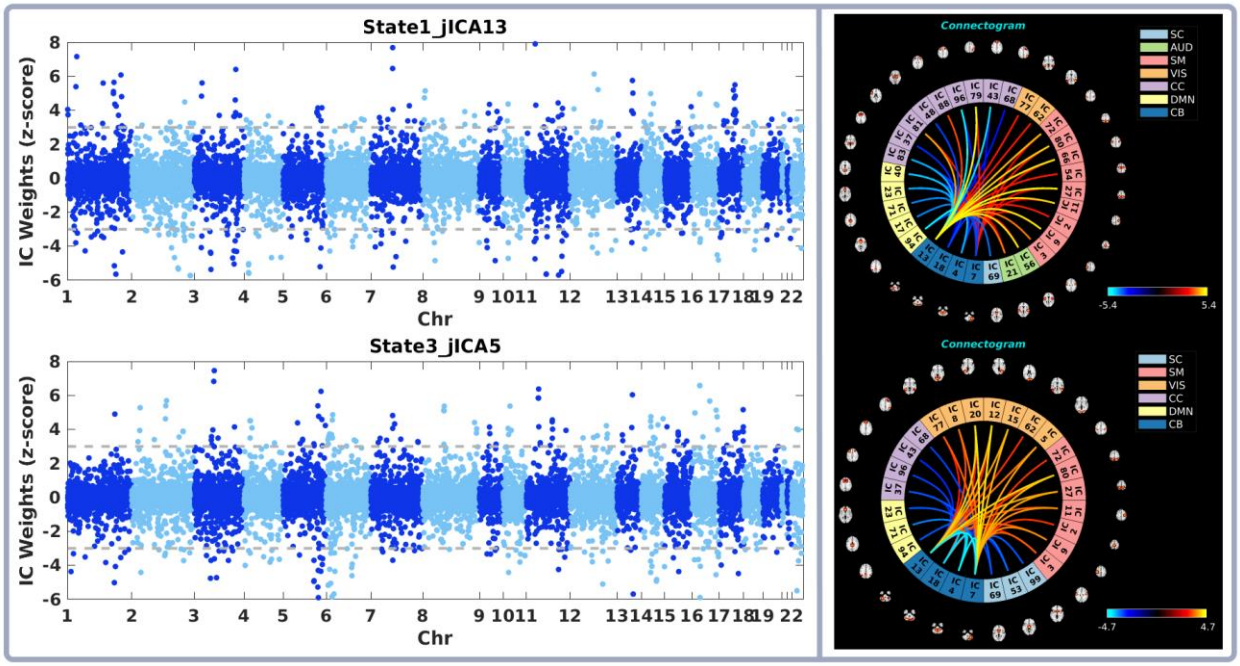

Figure 4: Manhattan and connectogram plots for State1_jICA13 (upper) and State3_jICA5 (lower), where dashed lines indicate |z-score| > 3.

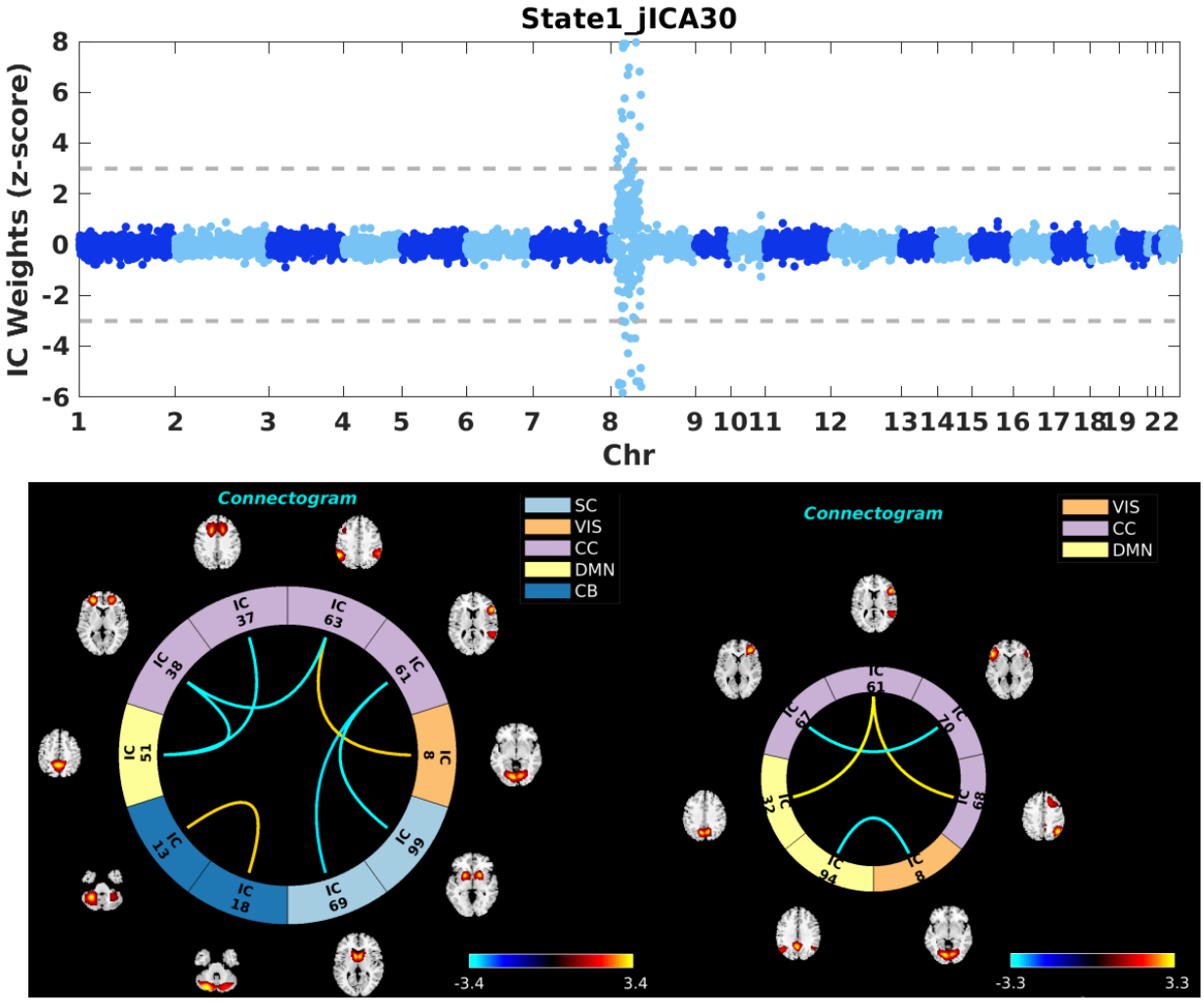

Figure 5: Manhattan and connectogram plots for State1_jICA30 (lower left) and State2_jICA32 (lower right), where dashed lines indicate |z-score| > 3.

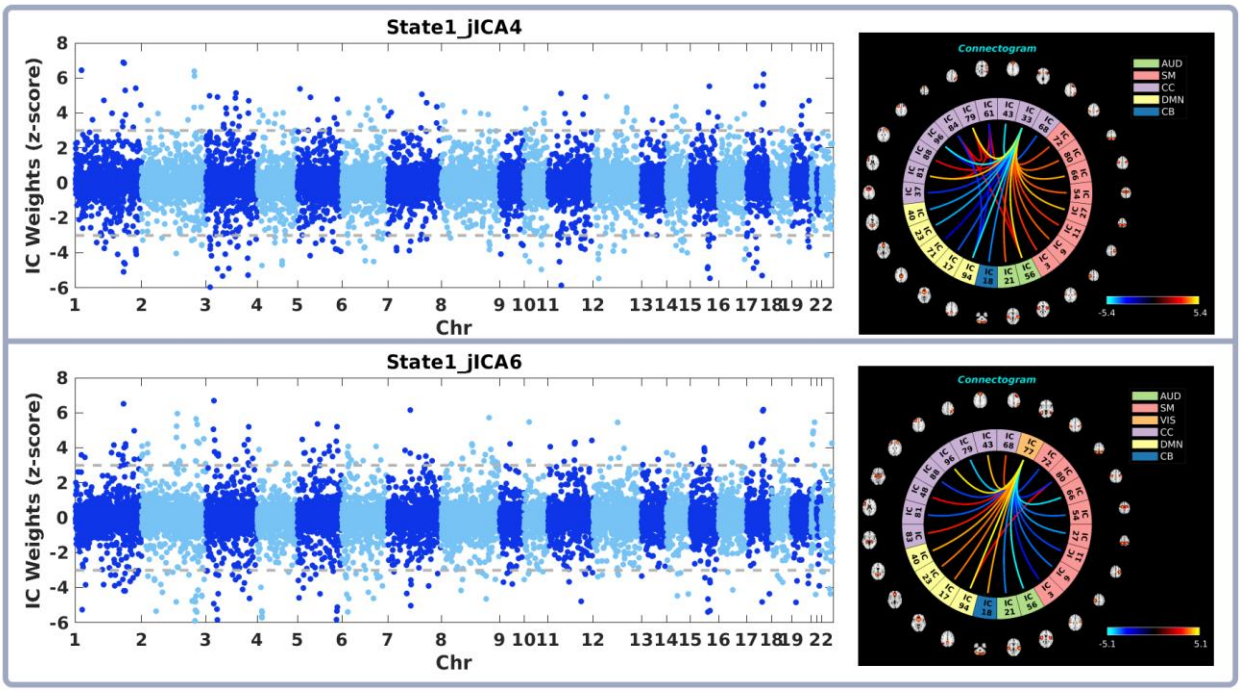

Figure 6: Manhattan and connectogram plots for State1_jICA4 (upper) and State1_jICA6 (lower), where dashed lines indicate |z-score| > 3.